Available online at www.sciencedirect.com
SCIENCE DIRECT®
Physics of the Earth and Planetary Interiors 145 (2004) 149–159
PHYSICS OF THE EARTH AND PLANETARY INTERIORS
www.elsevier.com/locate/pepi

Low-temperature olivine rheology at high pressure

Paul Raterron*, Yujun Wu, Donald J. Weidner, Jiuhua Chen

Department of Geosciences, Mineral Physics Institute, Stony Brook University, Stony Brook, NY 11794-2100, USA

Received 24 May 2002; accepted 17 March 2004

Abstract

San-Carlos olivine rheology was investigated at pressure (P) up to 9 GPa and temperature (T) lower than 890 °C. Six powder specimens were cold compressed and sintered into dense and compact materials, then deformed during relaxation experiments carried out at constant pressure and temperature in DIA-type cubic-anvil apparatus. Sample elastic strain was monitored during relaxation by in situ X-ray diffraction. Run product microstructures were characterized by transmission electron microscopy (TEM). A new method for measuring olivine rheology at high pressure from X-ray diffraction peak broadening is documented. From the data collected between 500 and 740 °C, the following rheological law is obtained:

$$\dot{\varepsilon}(s^{-1}) = 2.6\begin{pmatrix}+23\\-2.3\end{pmatrix} \times 10^{16} \times \exp\left\{-\frac{(564 \pm 89) \times 10^3}{RT(\mathrm{J/mol})}\left[1 - \left(\frac{\sigma(\mathrm{GPa})}{15.4 \pm 1.0}\right)^{2/3}\right]^2\right\},$$

where $\dot{\varepsilon}$ and σ are respectively the olivine microscopic plastic strain rate and internal stress, and R is the gas constant. TEM investigation of deformed sample microstructures reveals that this law corresponds to the activation of c-dislocation glide, and is thus representative of the olivine low-temperature dislocation-creep regime at high pressure.

Keywords: Olivine; Rheology; Low-temperature; High-pressure; X-ray diffraction; Microstructures

1. Introduction

Olivine, α-$(Mg,Fe)_2SiO_4$, is the main constituent of lithospheric materials sinking into the mantle in subduction zones. Its low-temperature ($T = 900$ °C) rheology controls the rheology of slabs in the upper mantle, where intermediate-focus earthquakes are observed to 370-km depth. Olivine shear instability was thus proposed in early studies (e.g., Griggs and Baker, 1969; Ogawa, 1987; Hobbs and Ord, 1988) as a possible mechanism responsible for these earthquakes, since at depth greater than typically 50–100 km pressure (typically higher than 3 GPa) prohibits brittle fracturing of rocks. Alternative mechanisms have been further proposed, such as a sudden dehydration of hydrous (altered) minerals (e.g., Meade and Jeanloz, 1991). Olivine shear instability, however, still remains a possible mechanism for the intermediate-focus earthquakes, especially for those occurring in the lower part of the double seismic zones observed in subducting slabs (e.g., Kao and Chen, 1995) where alteration by oceanic water is unlikely

* Corresponding author. Present address: Laboratoire de Structure et Propriétés de l'État Solide (Associated to CNRS), Université des Sciences et Technologies de Lille, F-59655, Villeneuve d'Ascq Cedex, France. Tel.: +33-320-43-46-86; fax: +33-320-43-65-91.
E-mail address: paul.raterron@univ-lille1.fr (P. Raterron).

0031-9201/$ – see front matter © 2004 Elsevier B.V. All rights reserved.
doi:10.1016/j.pepi.2004.03.007

to have occurred. Understanding the low-temperature rheology of olivine is thus critical for testing the possibility of such plastic instabilities.

Understanding the low-temperature rheology of olivine is also critical to better constrain olivine high-pressure transformations in slab (into β-phase and γ-phase). Indeed, the large volume reduction accompanying these transformations (6 and 8%, respectively) may generate in slabs high stress and large strain in the olivine surrounding the newly formed β and γ precipitates (Raterron et al., 2002). Such high stresses, generating defects in olivine, may enhance olivine transformation into its high-pressure polymorphs in the shallow transition zone, while the high-stress front propagates throughout the cold olivine, promoting its transformation at low temperature.

Despite its importance, olivine low-temperature rheology is poorly documented, mainly because the experimental approach raises technical difficulties. Olivine differential yield stress (σ_m = maximum σ_1–σ_3) is very high at low temperature, e.g., σ_m ~5 GPa at T ~100 °C (Evans and Goetze, 1979). At low pressure (typically $P < 300$ MPa), only indentation measurements can be performed without breaking apart specimens (Evans and Goetze, 1979; Gaboriaud et al., 1981; Darot et al., 1985). Although several attempts have been made to study olivine rheology at high pressure, they were until recently either limited to room temperature measurements (Meade and Jeanloz, 1990; Chai et al., 1998) or inaccurate in the determination of specimen yield stress and strain (Bussod et al., 1993; Karato and Rubie, 1997; a review in: Durham and Rubie, 1998).

We report here new results using a new method for investigating high-pressure low-temperature rheology in materials. San-Carlos olivine rheology was investigated at high pressure during relaxation experiments carried out in large-volume multi-anvil apparatuses, and monitored by in situ X-ray diffraction. The olivine microscopic elastic strain (ε_{el}) and strain rate ($\partial\varepsilon_{el}/\partial t$) were measured from the broadening of olivine diffraction peaks using the method reported by Weidner et al. (1994) (see also, Weidner et al., 1992a,b, 1998). Following Chen et al. (1998) and Weidner et al. (2001), the microscopic shear stress σ in olivine was deduced from ε_{el} using olivine elastic constants. Assuming a constant microscopic total strain (sum of both ε_{el} and plastic strain ε_{pl}), a usual assumption in relaxation experiments for which the loading pressure is maintained constant, the olivine plastic strain rate ($\dot{\varepsilon} = \partial\varepsilon_{pl}/\partial t$) was then deduced from $\partial\varepsilon_{el}/\partial t$, ultimately leading to olivine rheological law at low temperature (details in Wu, 2000, and below in Section 4).

2. Starting material and experimental procedure

Six San-Carlos olivine powder specimens (grain size <5–10 μm) were studied at high pressure in DIA-type cubic-anvil high-pressure apparatuses coupled with X-ray synchrotron radiation. Infrared (IR) measurements were carried out at the IR facilities (beam line U2A) of the NSLS (Upton, NY) on the centimeter-wide gem-quality single-crystals of San-Carlos olivine used as starting material. No appreciable IR absorption spectrum was observable after removing the scattering background. We thus estimate the starting-olivine bulk water content to less than 1 ppm wt. H_2O, which is the resolution at beam line U2A. After grounding of the starting material, the San-Carlos olivine powder was kept in an oven at 160 °C to prevent its hydration from atmospheric water before loading in the BN capsules inserted in the boron and epoxy pressure medium. All precautions were taken to prevent hydration of the starting material before the experiments. Although some atmospheric water may have entered the capsules during loading of the cell assemblies in the high-pressure apparatus, we believe that specimen water content was low during the experiments. Temperature was measured within ±10 °C using a W3%Re–W25%Re thermocouple situated next to the samples. The cell pressure (NaCl Decker's scale, see Decker, 1971) and the olivine microscopic elastic strain (crystal d-spacing distribution) were monitored by in situ X-ray diffraction (energy dispersive diffraction at 7.5° 2θ-angle) at the NSLS and the APS (Argonne, IL) synchrotron facilities. For each experiment, pressure was increased at room temperature to typically 9 GPa (Table 1). At high pressure (typically above 5 GPa), after compaction of the powder, samples became compact and dense material while their porosity was zero since hydrostatic pressure was higher than the olivine yield stress. Temperature was then increased by 50, 100, or 200 °C increments and maintained constant

Table 1
Run conditions

Run	Maximum P[a] (GPa)	Final T[b] (°C)	Duration (h:min)	Initial stress at final T (GPa)	TEM investigation
D0026	9.2	400	07:38	3.7	Yes
D0023	8.8	625	19:01	1.4	Yes
D0030	4.9	650	09:56	1.4	No
D0025	8.9	740	10:58	0.7	No
OLI02[c]	9.1	800	07:50	0.7	No
D0028	9.1	890	07:22	0.7	No

[a] Measured within 0.5 GPa after cold compression at room temperature.
[b] No pressure correction.
[c] Deformed previously by Weidner et al. (2001).

for 30 min to 10 h, or alternatively ramped up at a fixed and slow rate, while X-ray data were collected throughout the ramping process. We systematically waited long enough after each temperature step (typically 1000 s), or alternatively ramped the temperature at a slow enough rate, to ensure that sample characteristics (mainly peak broadening) were constant or nearly constant during X-ray data collection. This was also verified after the run while computing the data in terms of strain and stress. Samples were deformed with temperature in excess to 650 °C and up to 890 °C for some samples, except for samples D0023 and D0026 quenched respectively at 625 and 400 °C in order to investigate the corresponding microstructures by TEM. Specimens for TEM were cut in optically selected areas of doubly polished petrographic sections (~25 μm thick) prepared from the center of the run products. Petrographic sections were then ion-thinned with a 5 kV argon beam to electron transparency, then carbon coated. A Philips CM30 and a Jeol 200CX electron microscope, operating respectively at 300 and 200 kV, were used to investigate the specimens.

3. In situ X-ray diffraction and corresponding microstructures

The X-ray diffraction peak-broadening method is widely used in materials science to determine strain and stress in metals and alloys (e.g., Westwood et al., 1995). It was introduced in Earth-science high-pressure research in the early 1990s (Weidner et al., 1992a,b). Grain boundary contacts in loose packed powder along with elastic anisotropy generate an internal microscopic stress field when polycrystalline samples are under hydrostatic pressure. This stress field persists in the dense (non-porous) high-pressure material and promotes microscopic elastic strain, which in turn contributes to the broadening of sample diffraction peaks. By measuring this broadening and separating the different contributions (instrumental broadening, elastic-strain and grain-size broadening) it is possible to quantify the microscopic elastic strain (ε_{el}) in the sample, as well as the average grain size for grains smaller than typically 150 nm (e.g., Willets, 1965; Gerward et al., 1976). The microscopic shear stress (σ) is then obtained by multiplying ε_{el} by the Young's modulus (E) (details in: Chen et al., 1998; Wu, 2000; Weidner et al., 2001).

Fig. 1 shows the maximum differential stress (yield stress σ_m, twice the shear stress) measured in sample OLI02 and D0030 versus temperature. Superimposed to these data, are the data reported for olivine by Evans and Goetze (1979) (room pressure, hardness-derived yield stress) and Meade and Jeanloz (1990) (8 GPa, sample momentum-balance derived yield stress). Fig. 1 shows that, despite different experimental techniques and data collection methods, our results are in good agreement with previous works. Comparing our data to Evans and Goetze's (1979) data, we do not observe a significant increase of σ_m with increasing pressure over a 9 GPa pressure range, as was reported on a wider range of pressure (Meade and Jeanloz, 1990; Chai et al., 1998).

We systematically observed two different deformation regimes separated by a rapid decrease of σ_m occurring at about 450–500 °C. This rapid stress drop is illustrated in Fig. 2, which shows olivine differential stress versus temperature and time, as measured in samples D0026 and D0023. Differential stress is in

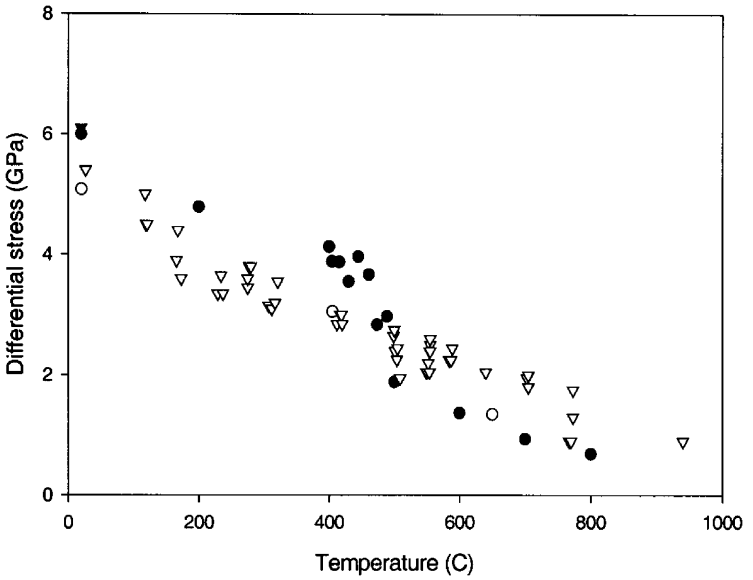

Fig. 1. Differential yield stress σ_m in olivine vs. temperature, as measured by in situ X-ray diffraction during runs Oli02 (9.2 GPa, solid circle) and D0030 (4.9 GPa, open circle). Superimposed to our data are Evans and Goetze's (1979) data (room pressure, open triangle) and Meade and Jeanloz's (1990) data (8 GPa, solid triangle).

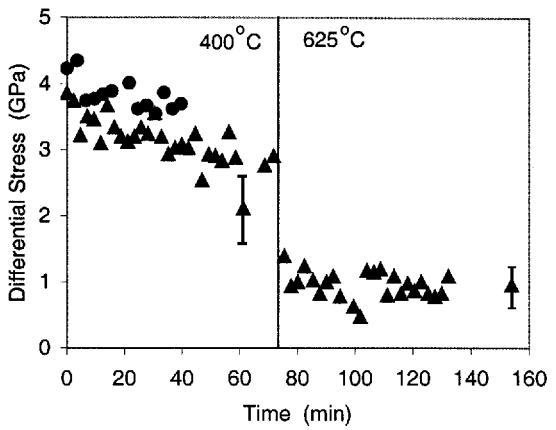

Fig. 2. Differential stress in olivine vs. temperature and time, as measured in samples D0023 (solid triangles) and D0026 (solid circles), quenched respectively at 625 and 400 °C (Table 1). The two error bars show typical uncertainties in stress measurements at each temperature. The major source of uncertainty is the experimental error in diffraction peak broadening measurements. We used first order error propagation to estimate the stress uncertainty. A rapid stress drop event is systematically observed in our samples in the range 450–500 °C.

excess of 3 GPa in both samples at 400 °C, and drops to about 1 GPa or less at 625 °C in sample D0023. Such a rapid stress drop event was also observed in dry olivine by Chen et al. (1998) (their Fig. 2). This rapid stress drop event is accompanied by macroscopic deformation of the samples. Fig. 3 shows photographs of samples D0026 and D0023 cross-sections after the runs. The olivine-salt interface in sample D0026 is still approximately flat at 400 °C, as it was initially before the run, while it exhibits a distinctive parabolic-like shape at 625 °C in sample D0023.

The rapid stress drop event also corresponds to critical changes in sample microstructures. At 400 °C, olivine exhibits an average grain size lower than typically 100 nm, as revealed by in situ X-ray diffraction (Fig. 4). This nanometric texture develops during sample cold compression, likely at low pressure by nano-cracking (possibly along cleavage planes) of the olivine powder. TEM investigation of olivine microstructures at 400 °C confirms the X-ray diffraction data (Fig. 5A), and shows nanometric sub-domains (typically 50-nm in size) in the olivine grains. Such a cataclastic grain size reduction during cold compression has been previously observed in forsterite powder samples (Brearley et al., 1992). At 625 °C,

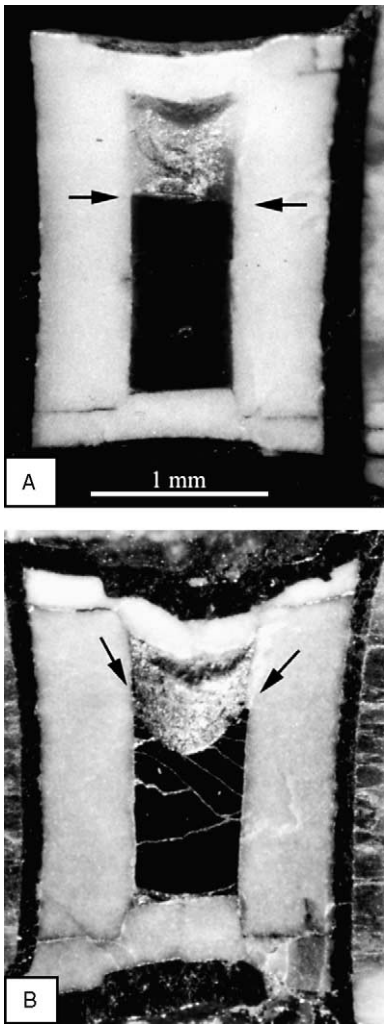

Fig. 3. Photographs of two cell-assembly sections after runs (A) D0026 and (B) D0023, quenched respectively at 400 and 625 °C. The olivine specimens appear in dark grey, in the center of each picture, surrounded by the white BN capsule. The cracks visible in sample D0023 probably occurred during decompression at room temperature. The NaCl pressure calibrant, which has been dissolved during the section preparation, left the empty spaces above both olivine specimens. The positions of olivine-salt interfaces are indicated (arrows).

olivine exhibits a very different texture, with grain sizes ranging from 0.5 to 5 μm (Fig. 5B). From the TEM investigation of sample D0023, we estimate that at 625 °C more than 50% of the sample volume corresponds to grains larger than 1 μm in diameter. Olivine grains in sample D0023 also exhibit numerous *c*-dislocations with screw segments extending throughout the grains (Fig. 5C) and edge segments forming tangle-like features in the vicinity of grain boundaries. This indicates that *c* glide, particularly the glide of edge dislocations, was a dominant deformation mechanism above 500 °C in our samples. This observation is in good agreement with previous studies of experimentally-indented and naturally-deformed olivine, which shows that [0 0 1]{1 1 0} slip systems are dominant systems in the range 500 °C < *T* < 900 °C (e.g., Evans and Goetze, 1979; Mercier, 1985). The (0 1 0) glide plane was also previously characterized for *c*-dislocation in San-Carlos olivine powder specimens deformed at high pressure between 700 and 1000 °C, after experiencing similar *P*–*T* paths to that of our samples (Li et al., 2003). This result together with our TEM observations suggest that the [0 0 1](0 1 0) dislocation slip system, active at high temperature, was also active above 500 °C in our experiments. From the microstructures observed in our sample by TEM, the active deformation mechanism in the range 500–890 °C is identified as obstacle/Peierls' stress limited dislocation creep.

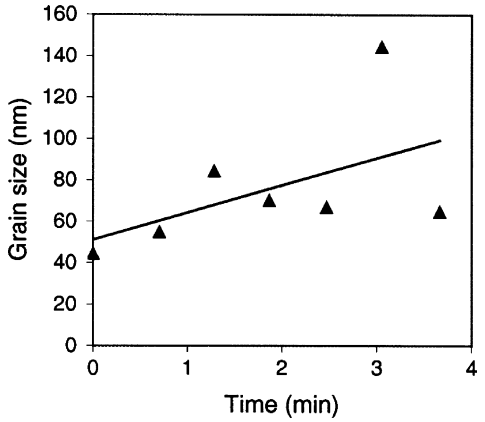

Fig. 4. Olivine average grain size vs. time, as measured by in situ X-ray diffraction at 400 °C in sample D0026. After about 2 min, the grain size becomes larger than typically 100–150 nm, and the peak-broadening method becomes inappropriate for measuring grain size, as shown by the experimental-point discrepancy. Reduction in the high density of defects induced by cold compression, and of the high surface energy of the nanometric grains or sub-domains, is probably a strong enough driving force for promoting olivine grain growth at low temperature.

The observations reported above suggest that the rapid stress drop event observed in our samples at

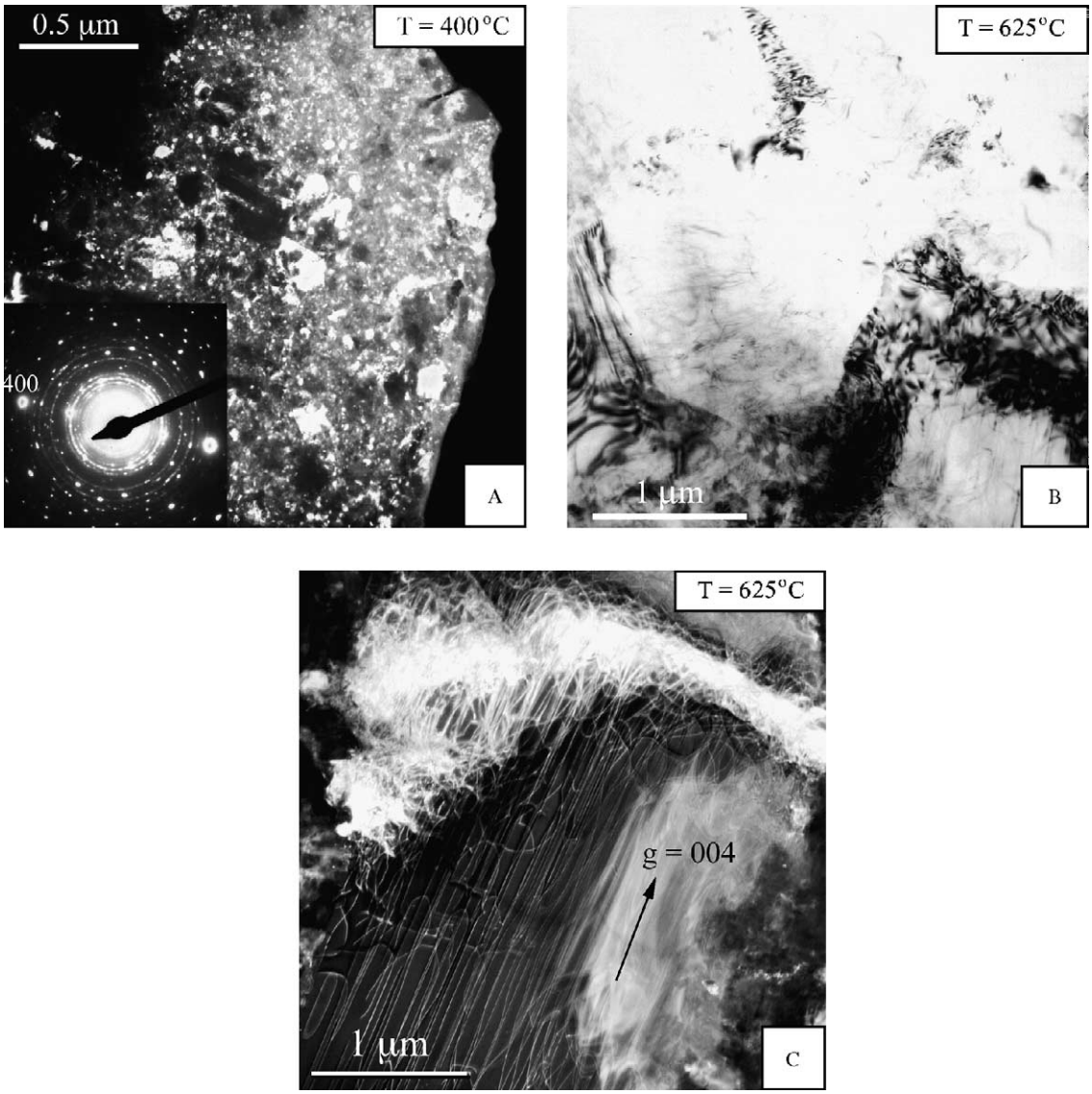

Fig. 5. TEM micrographs of olivine run products. (A) Dark field micrograph showing nanometric sub-domains in an olivine grain at 400 °C in sample D0026. The nanometric texture probably results from nano-cracking during cold compression of the specimen. The inset shows the corresponding diffraction pattern. (B) Bright field micrograph showing large (micrometric) restored olivine grains at 625 °C in sample D0023. The dark contrasts appearing in the vicinity of grain boundaries result from electron scattering due to high dislocations densities in these regions. (C) Dark field weak beam micrograph of sample D0023 quenched at 625 °C, showing high density of *c*-dislocations. Dislocation screw segments extend throughout olivine grains, while the active edge segments form tangle-like features in the vicinity of grain boundaries.

about 450–500 °C corresponds to a restoration event in an extremely defective olivine. Consequently, the X-ray data collected below this temperature are not representative of natural olivine deformation and will not be further discussed. Conversely, the data collected in the range 500–890 °C are representative of natural deformations in slabs, since the restoration event erases the sample cold compression history

(nanometric texture) and allows the activation of the *c* glide, a mechanism characteristic of low-temperature deformation in olivine. We interpret these data in terms of rheological law in the following section.

4. Olivine low-temperature rheological law at high pressure

The relaxation process following each temperature increment above 500 °C, was quite fast at first, then slowed down with increasing relaxation time. Correspondingly, the strain rate decreased with relaxation time. From the slope of the strain and time, we obtained strain rates ranging from 10^{-5} to $10^{-8}\,s^{-1}$. However, above typically 750 °C, stresses and elastic strains became small (less than a few hundreds MPa). As a consequence, in situ rheological measurements became inaccurate with increasing temperature, and above 750 °C not accurate enough for inferring rheological laws. Since the X-ray data obtained below 500 °C are not representative of natural deformation (see previous section), we thus only used the data collected in the range 500–740 °C to deduce the olivine low-temperature rheological law. Our TEM observations suggest, however, that the corresponding rheological law applies to higher temperature, since the obstacle/Peierls' stress limited dislocation creep regime appears to dominate olivine deformation up to 890 °C.

We would like to emphasize here that steady-state deformation conditions were obviously not achieved during data collection in our experiments, since data were collected during relaxation of the specimen, i.e., with constantly decreasing stress and strain rate. In traditional deformation experiments, constant strain rate and stress conditions (steady-state conditions) are achieved in order to match the external stress applied to the sample to the (assumed) homogeneous average stress field within the sample. Steady-state conditions also ensure that sample-defect populations (mobile dislocation density, point-defect concentrations) reached equilibrium, i.e., are homogeneous throughout the volume of the sample. In our experiments no external stress was applied, and both the local internal stress (always heterogeneous in heterogeneous materials) and the corresponding microscopic elastic strain were measured simultaneously, within the same small area in the sample. Time to reach local equilibrium between internal stress and mobile dislocation density was thus at the local scale much shorter than that necessary to reach equilibrium throughout a sample experiencing an externally applied stress. As much as possible, our data were collected after a delay ensuring that sample peak broadening was not changing significantly during data collection. This delayed local and simultaneous measurement ensures that for each data point the measured strain and stress are representative of nearly equilibrated local defect population, which allows the interpretation of our data in terms of "steady-state" rheological law despite non-steady-state condition.

At given T and P condition, the microscopic elastic strain (ε_{el}) was obtained at each temperature as a function of time (t) from the broadening of sample X-ray diffraction peaks. Because of some scattering in the X-ray data (e.g., Fig. 2), we fitted them to a smooth function between ε_{el} and time (t). We then differentiated this function to obtain the elastic strain rate ($\partial\varepsilon_{el}/\partial t$) as a function of time. Assuming a constant microscopic total strain (elastic + plastic) during relaxation, the microscopic plastic strain rate ($\dot{\varepsilon}$) is simply:

$$\dot{\varepsilon} = \frac{\partial \varepsilon_{pl}}{\partial t} = -\frac{\partial \varepsilon_{el}}{\partial t} \tag{1}$$

By measuring the microscopic shear stress ($\sigma = E\varepsilon_{el}$) and strain rate ($\dot{\varepsilon}$) at each P–T–t conditions, it was thus possible to analyze the data in terms of rheological laws. We used Bass's (1995) parameters to calculate olivine Young's modulus E at each P–T condition.

TEM investigation of olivine microstructures shows evidences of obstacle/Peierls' stress limited dislocation-glide deformation regime at $T > 500$ °C, further called dislocation creep regime for simplicity. Considering the high stresses applied on the specimens at low temperature, the appropriate rheological law to interpret our data reads (see also Evans and Goetze, 1979):

$$\dot{\varepsilon} = \dot{\varepsilon}_0 \exp - \frac{(F_0[1 - (\sigma/\tau)^p]^q)}{RT} \tag{2}$$

where $\dot{\varepsilon}_0$ is a pre-exponential constant, and where the dependence on σ is expressed through the exponential term which is function of F_0, the free energy for the dislocations to overcome friction and obstacles

(sometimes refers as activation energy), and τ the maximum glide resistance which quantifies the Peierls' stress, as well as the two fitting parameters p and q. Theoretical considerations set the values for p and q in the ranges: $0 \leq p \leq 1$, and $1 \leq q \leq 2$ (e.g., Frost and Ashby, 1982). Note that no activation volume appears in Eq. (2). Instead, the pressure effect on olivine rheology appears indirectly in Eq. (2) through the parameter τ, since an increase of P is expected to promote an increase of the Peierls' stress, as evidenced further.

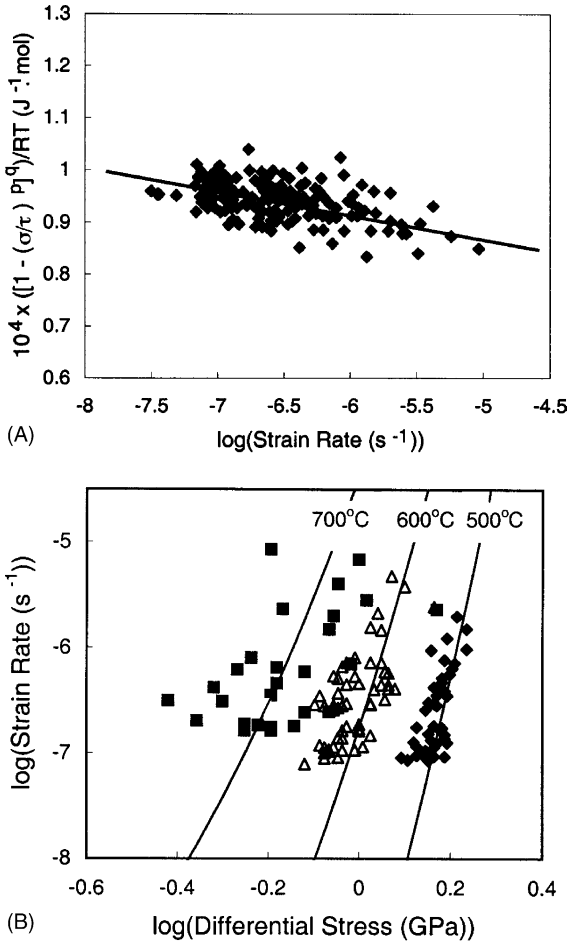

Fig. 6. (A) $\mathrm{Log}_{10}(\dot{\varepsilon})$ vs. $([1-(\sigma/\tau)^p]^q)/RT$ (see Eq. (3)) as measured in sample OLI02 between 500 and 740 °C. We used $p = 2/3$ and $q = 2$ for this plot. The solid line shows the linear relationship in (Eq. (3)) corresponding to the best fit for parameters F_0 and τ (respectively 564 kJ/mol and 15.4 GPa) using all available data above 500 °C. (B) $\mathrm{Log}_{10}(\dot{\varepsilon})$ vs. $\log_{10}(s)$, as measured in situ in sample OLI02 at 500, 600 and 700 °C. The solid line shows the best fitted rheological law corresponding to the parameters reported in Table 2. Note that the X-ray diffraction peak-broadening method become inaccurate in relaxation experiment above 700 °C, since differential stresses become very small.

Eq. (2) can be rewritten in a non-dimensional form:

$$\ln\left(\frac{\dot{\varepsilon}}{\dot{\varepsilon}_o}\right) = -\frac{F_0 \times [1-(\sigma/\tau)^p]^q}{RT} \quad (3)$$

Fitting σ and T at given strain rate $\dot{\varepsilon}$ using a least-square method leads to the determination of the parameters p, q, and τ. We obtained the best fit with $p = 2/3$ and $q = 2$, which results in $\tau = 15.4 \pm 1.0$ GPa. The uncertainty on τ was estimated by adjusting the values of τ to fit the experimental data as explained below. With the above set of p, q and the estimation on the τ parameters, values for F_0, and $\dot{\varepsilon}_0$ parameters were obtained by fitting at best our data using Eq. (2), as illustrated in Fig. 6. We obtained $F_0 = 564 \pm 89$ kJ/mol. F_0 and $\dot{\varepsilon}_0$ values were determined by fitting the data to a linear equation for a given τ value as shown in Fig. 6A, and by plotting the resulting rheological law in Fig. 6B and comparing it to the data. Using an iterative protocol between the plots illustrated in Fig. 6A and B, we determined the values and uncertainties for the τ, F_0, and $\dot{\varepsilon}_0$ parameters. The p, q, τ, F_0, and $\ln(\dot{\varepsilon}_0)$ values resulting from the best fit of our 500–740 °C data using Eq. (2) are listed in Table 2 (see also Fig. 6B). We did not observe any significant variation of these parameters with strain rate. The values reported by Evans and Goetze (1979) for the same set of parameters over a comparable temperature range (350–950 °C) also appear in Table 2 for comparison.

5. Discussion

The data we obtain for olivine, in particular the yield stress values, compare well with previous data obtained for olivine at low temperature (see Fig. 1), yet we observed a rapid stress drop at 450–500 °C that was not reported previously. We interpret this stress drop as resulting from a rapid restoration event in a defective although dense olivine (see above). From the data obtained at $T \geq 500$ °C, we deduced the parameters (Table 2) for the rheological law presented in Eq. (2), which are representative of low-temperature olivine rheology. These parameters are discussed below.

Table 2
Resulting parameters for Eq. (2)

T range (°C)	p	q	$\ln(\dot{\varepsilon}_0$ (s^{-1}))	F_0 (kJ/mol)	τ (GPa)
500–740	2/3	2	37.8 ± 2.3[a]	564 ± 89[a]	15.4 ± 1.0[a]
350–950[b]	1	2	27.8934	502	9.1

[a] 1σ standard deviation.
[b] Evans and Goetze (1979) room P.

Among the parameters reported in Table 2, we can distinguish between the fitting parameters p, q, and $\ln(\dot{\varepsilon}_0)$, and the parameters F_0 and τ whose physical significance is more direct. Both sets of parameters in Table 2 compare well, given the different pressure-ranges and investigation techniques of the two studies. The observed difference in $\dot{\varepsilon}_0$ values is not significant, since it mainly results from the "leverage" effect of a small activation-energy difference extrapolated to infinite temperature ($1/T \rightarrow 0$, see Eq. (2)). The value we obtain for F_0, although slightly higher than that reported by Evans and Goetze (1979), agrees well with previously reported activation energy values for dislocation creep in dry olivine, e.g., Chopra and Paterson (1984) report 535 kJ/mol for dry dunite deformation, and Bai et al. (1991) report 540 kJ/mol for the activation of *c*-dislocation slip system in opx-buffered olivine single crystals. This confirms our TEM observations evidencing the dislocation-creep regime above 500 °C and the activation of the *c*-dislocation glide during our experiments. It also gives us confidence in the new X-ray diffraction rheological method presented here.

Another interesting observation is the significant increase of τ with increasing pressure. As previously mentioned, the parameter τ is much related to the Peierls' stress, which is the minimum stress dislocations need to overcome the lattice resistance and glide in their respective plane. An increase of the Peierls' stress, here corresponding to the *c*-dislocation glide planes, would result in an increase of τ in Eq. (2). From experiments carried out at room pressure, at comparable temperature and stress level to those in our experiments, Evans and Goetze (1979) report $\tau = 9.1$ GPa. We measured $\tau = 15.4$ GPa at about 9 GPa pressure, which represents a relative increase of τ of almost 70%. Although never measured directly, an increase of the flow stress with pressure is expected to occur in most crystals, and was indeed indirectly observed in numerous materials including metals and alkali halide (a review in: Poirier, 1985, pp. 153–154). Such an increase is generally attributed to the increase in the stress needed to overcome obstacles, mostly because of the corresponding increase in the elastic shear modulus. An observed increase of the flow stress with pressure in pure nickel, an order of magnitude greater than the modulus increase (Jesser and Kuhlmann-Wilsdorf, 1972), has also directly been attributed to a Peierls' stress pressure dependence, which was in turn attributed to the dilatation and contraction of dislocation cores (breathing core effect) while dislocations move from one Peierls' valley to another. Similarly, and increase in the Peierl's stress has been recently calculated (atomistic calculation) for screw dislocation in bcc tantalum (e.g., Yang et al., 2001). Yang et al. (2001) report that the pure-shear Peierls' stress should scale linearly with the pressure-dependent ⟨1 1 1⟩ bcc-tantalum shear modulus. In olivine, the C_{44} elastic constant corresponds to glide along the *c* direction in the (0 1 0) plane, an active slip system characterized in our samples (see above). Using the data reported by Kumazawa and Anderson (1969), we find that in San-Carlos olivine C_{44} increases from 64.6 GPa at room pressure to 84.1 GPa at 9 GPa, i.e., C_{44} increases by about 30% over the 9 GPa pressure range, which is less than half the relative increase we estimated for the τ parameter over the same pressure range. This relatively large increase of the τ parameter, if confirmed by further studies, may also reflect an increase of the Peierls' stress with pressure, possibly due to an effect of expanded *c*-dislocation core in olivine.

6. Conclusion

The present work shows that, assuming a constant total microscopic strain (elastic + plastic) during relaxation—a reasonable assumption above 450 °C in

the framework of these experiments—and after careful investigation of run-product microstructures, it is now possible to measure material rheological laws at high pressure from in situ X-ray diffraction experiments. The diffraction-peak broadening method we apply here in relaxation experiments on compacted and dense powder olivine specimens is limited to low temperature data collection, since it requires high stresses (typically of a few hundreds MPa) which tend to vanish at high temperature. It is, however, an efficient method for investigating Earth-material rheology, in particular olivine rheology, in the high-pressure low-temperature geological context of subducting slabs. The low-temperature high-pressure olivine rheological law we report (Eq. (2) and Table 2) does not differ strongly from the one obtained at room pressure, although pressure seems to promote a significant increase of the dislocation-plane Peierls' stress, here observed (indirectly) for the first time in olivine.

Acknowledgements

This work was supported by the Center for High Pressure Research [CHiPR is a NSF Science and Technology Center], NSF Grant EAR-9909413, and the Centre National de la Recherche Scientifique (CNRS). Research was carried out (in part) at the NSLS and APS, synchrotron facilities supported by the US Department of Energy, under Contract No. DE-AC02-98CH10886 and W-31-109-Eng-38. We are grateful for the assistance of Z. Liu and L. Wang for the I.R. measurements, and the help of M. Vaughan, Z. Zhong, Y. Wang and T. Uchida at the beamlines, as well as for the suggestions of two anonymous reviewers to improve the manuscript. This is the MPI contribution # 349.

References

Bai, Q., Mackwell, S.J., Kohlstedt, D.L., 1991. High-temperature creep of olivine single crystals, 1, mechanical results for buffered samples. J. Geophys. Res. 96, 2441–2463.

Bass, J.D., 1995. Elasticity of minerals, glasses and melts. In: Ahrens T.J. (Ed.), Handbook of Physical Constants: Mineral Physics and Crystallography. American Geophysical Union Ref., Shelf Series 2, pp. 45–63.

Brearley, A.J., Rubie, D.C., Ito, E., 1992. Mechanisms of the transformations between the α, β, and γ polymorphs of Mg_2SiO_4 at 15 GPa. Phys. Chem. Miner. 18, 343–358.

Bussod, G.Y., Katsura, T., Rubie, D., 1993. The large volume multi-anvil press as a high *P–T* deformation apparatus. Pure Appl. Geophys. 141, 579–599.

Chai, M., Brown, M., Wang, Y., 1998. Yield strength, slip systems and deformation induced phase transition of San-Carlos olivine up to the transition zone pressure at room temperature. In: Manghnani, M.H., Yagi, T. (Eds.), Properties of Earth and Planetary Materials. American Geophysical Union, Geophysical Monograph Series 101, pp. 483–493.

Chen, J., Inoue, T., Weidner, D.J., Wu, Y., Vaughan, M.T., 1998. Strength and water weakening of mantle minerals, olivine, wadsleyite and ringwoodite. Geophys. Res. Lett. 25, 575–578.

Chopra, P.N., Paterson, M.S., 1984. Therole of water in the deformation of dunite. J. Geophys. Res. 89, 7861–7876.

Darot, M., Gueguen, Y., Benchemam, Z., Gaboriaud, R., 1985. Ductile-brittle transition investigation by micro-indentation: results for quartz and olivine. Phys. Earth Planet. Int. 10, 180–186.

Decker, D.L., 1971. High-pressure equations of state for NaCl, KCl, and CsCl. J. Appl. Phys. 42, 3239–3244.

Durham, W.B., Rubie, D.C., 1998. Can the multianvil apparatus really be used for high-pressure deformation experiments? In: Manghnani, M.H., Yagi, T. (Eds.), Properties of Earth and Planetary Materials at High Pressure and Temperature, Geophysical Monograph 101, American Geophysical Union, Washington, pp. 63–70.

Evans, B., Goetze, C., 1979. The temperature variation of hardness of olivine and its implication for polycrystalline yield stress. J. Geophys. Res. 84, 5,505–5,524.

Frost, H.J., Ashby, M.F., 1982. Deformation-Mechanism Maps, The Plasticity and Creep of Metal and Ceramics, Pergamon Press.

Gaboriaud, R.J., Darot, M., Gueguen, Y., Woirgard, J., 1981. Dislocations in olivine indented at low temperature. Phys. Chem. Miner. 7, 100–104.

Gerward, L., Mørup, S., Topsøe, H., 1976. Particle size and strain broadening in energy-dispersive X-ray powder patterns. J. Appl. Phys. 47, 822–825.

Griggs, D.T., Baker, D.W., 1969. The Origin of deep-focus earthquakes. In: Mark, H., Fernbach, S. (Eds.), Properties of matter under unusual conditions, Interscience Publishers, New York/London/Sydney/Toronto, pp. 23–42.

Hobbs, B.E., Ord, A., 1988. Plastic instabilities: implications for the origin of intermediate and deep focus earthquakes. J. Geophys. Res. 93, 10,521–10,540.

Jesser, W.A., Kuhlmann-Wilsdorf, D., 1972. The flow stress and dislocation structure of nickel deformed at very high pressure. Mater. Sci. Eng. 9, 111–117.

Kao, W.P., Chen, H., 1995. Transition from interplate slip to double seismic zone along the Kuril-Kamchatka arc. J. Geophys. Res. 100, 9,881–9,903.

Karato, S., Rubie, D., 1997. Toward an experimental study of deep mantle rheology: a new multianvil sample assembly for deformation studies under high pressures and temperatures. J. Geophys. Res. 102, 20,111–20,122.

Kumazawa, M., Anderson, O.L., 1969. Elastic moduli, pressure derivatives, and temperature derivatives of single-crystal olivine and single crystal forsterite. J. Geophys. Res. 74, 5961–5972.

Li, L., Raterron, P., Weidner, D.J., Chen, J., 2003. Olivine Flow mechanisms at 8 GPa. Phys. Earth Planet. Int. 97, 121–131.

Meade, C., Jeanloz, R., 1990. The strength of mantle silicates at high pressure and room temperature: implications for the viscosity of the mantle. Nature 348, 533–535.

Meade, C., Jeanloz, R., 1991. Deep-focus earthquakes and recycling of water into the Earth's mantle. Science 252, 68–72.

Mercier, J.C.C., 1985. Olivine and pyroxenes. In: Wenk, H. (Ed.), Preferred Orientation in Deformed Metals and Rocks: An Introduction to Modern Texture Analysis. Academic Press, Orlando, FL, pp. 407–430.

Ogawa, M., 1987. Shear instability in a viscoelastic material as the cause of deep focus earthquakes. J. Geophys. Res. 92, 13,801–13,810.

Poirier, J.P., 1985. Creep of crystals. In: Cook, A.H., Harland, W.B., Hughes, N.F., Putnis, A., Sclater, J.G., Thomson, M.R.A. (Eds.), Cambridge Earth Science Series. Cambridge University Press, Cambridge, New York, Melbourne, pp. 153–154.

Raterron, P., Chen, J., Weidner, D.J., 2002. A process for the low-temperature olivine-spinel transition under quasi-hydrostatic stress. Geophys. Res. Lett. 29 (10), 361–364.

Weidner, D.J., Vaughan, M.T., Ko, J., Wang, Y., Leinenweber, K., Liu, X., Yeganeh-Haeri, A., Pacalo, R.E., Zhao, Y., 1992a. Large volume high pressure research using the wiggler port at NSLS. High Pressure Res. 8, 617–623.

Weidner, D.J., Vaughan, M.T., Ko, J., Wang, Y., Liu, X., Yeganeh-Haeri, A., Pacalo, R.E., Zhao, Y., 1992b. Characterization of stress, pressure, and temperature in SAM-85, a DIA type high pressure apparatus. In: Syono, Y., Manghnani, M. (Eds.) Proceedings of the US Japan High Pressure Conference. Terra Scientific Publishing Co., Tokyo, pp. 13–17.

Weidner, D.J., Wang, Y., Ando, J., Vaughan, M.T., 1994. Yield stress at high pressure and temperature. Geophys. Res. Lett. 21, 753–756.

Weidner, D.J., Wang, Y., Chen, G., Ando, J., Vaughan, M.T., 1998. Rheology measurements at high pressure and temperature. In: Manghnani, M.H., Yagi, T. (Eds.), Properties of Earth and Planetary Materials at High Pressure and Temperature. American Geophysical Union, Geophysical Monographs 101, pp. 473–482.

Weidner, D.J., Chen, J., Xu, Y., Wu, Y., Vaughan, M.T., Li, L., 2001. Subduction zone rheology. Phys. Earth Planet. Int. 127, 67–81.

Westwood, A.D., Murray, C.E., Noyan, I.C., 1995. In-situ study of dynamic structural rearrangements during stress relaxation. Adv. X-ray Anal. 38, 243–254.

Willets, F.W., 1965. An analysis of X-ray diffraction line profiles using standard deviation as a measure of breadth. Br. J. Appl. Phys. 16, 323–333.

Wu, Y., 2000. Rheological Studies of Olivine under High Pressure and Temperature. Ph.D. thesis dissertation. State University of New York at Stony Brook, NY, USA.

Yang, L.H., Söderlind, P., Moriaty, J.A., 2001. Atomistic calculation of pressure-dependent screw dislocation properties in bcc tantalum. Mater. Sci. Eng. A 309–310, 102–107.